

Are There Three Peaks in the Power Spectra of GX 339–4 and Cyg X-1?

M.A. Nowak¹

¹ JILA, University of Colorado, Campus Box 440, Boulder, CO 80309-0440, U.S.A.

29 October 2018

ABSTRACT

Among the variability behaviour exhibited by neutron star systems are the so-called “horizontal branch oscillations” (HBO, with frequencies ≈ 50 Hz), the “lower-frequency kHz quasi-periodic oscillation” (QPO) and the “upper-frequency kHz QPO”, with the latter two features being separated in frequency by an amount comparable to, but varying slightly from, the suspected spin-frequency of the neutron star. Recently, Psaltis, Belloni, & van der Klis (1999) have suggested that there exists a correlation between these three frequencies that, when certain identifications of variability features are made, even encompasses black hole sources. We consider this hypothesis by reanalyzing a set of GX 339–4 observations. The power spectral density (PSD) constructed from a composite of 7 separate, but very similar, observations shows evidence for three broad peaks in the PSD. If the peak frequencies of these features are identified with “QPO”, then their frequencies approximately fit the correlations suggested by Psaltis, Belloni, & van der Klis (1999). We also reanalyze a Cyg X-1 observation and show that the suggested QPO correlation may also hold, but that complications arise when the “QPOs” (which, in reality, are fairly broad features) are considered as a function of energy band. These fits suggest the existence of at least three separate, independent physical processes in the accretion flow, a hypothesis that is also supported by consideration of the Fourier frequency-dependent time lags and coherence function between variability in different energy bands. If these variability features have a common origin in neutron star and black hole systems, then “beat frequency models” of kHz QPO in neutron star systems are called into question.

Key words: accretion — black hole physics — Stars: binaries — X-rays:Stars

1 INTRODUCTION

Observations by the *EXOSAT* and later by the *Ginga* satellites during 1980’s and early 1990’s, and more recently by the *Rossi X-ray Timing Explorer (RXTE)* have revealed a rich variety of X-ray variability behaviour in neutron star and black hole candidate (BHC) systems. Neutron star systems in general, and the so-called Z-sources in specific (Hasinger & van der Klis 1989), have exhibited a set of relatively narrow features in their X-ray variability power spectral densities (PSD). These features, referred to as quasi-periodic oscillations (QPO), phenomenologically appear to fall predominantly into one of four classes. At low Fourier frequencies (see van der Klis 1995 for a review) there are the so-called normal branch oscillations (NBO) with $f \approx 5$ –20 Hz and the horizontal branch oscillations (HBO) with $f \approx 15$ –60 Hz. A second set of QPO, typically occurring in pairs at high frequencies $f \approx 200$ –1200 Hz, are referred to as the “lower-frequency kHz QPO” and the “upper-frequency kHz QPO” (van der Klis et al. 1996). Similar high frequency fea-

tures have been observed in lower-luminosity neutron star systems, specifically the so-called atoll sources (Strohmayer et al. 1996). The atoll systems also have exhibited low-frequency features that in some ways are similar to the HBO (see Hasinger & van der Klis 1989, Homan et al. 1998).

A wide variety of features ranging from narrow (see, for example, Nowak, Wilms, & Dove 1999; hereafter NWD) to broad “noise components” (see, for example, the discussion of van der Klis 1994a, van der Klis 1994b) have been observed in BHC systems as well. Frequently, the PSDs associated with these systems are flat at low frequencies, show a low frequency break into a steeper f^{-1} – f^{-2} spectrum, and often exhibit a low frequency QPO at frequencies slightly above the break (see Wijnands & van der Klis 1999, and references therein). It has been noted that the location of the break and the frequency of the QPO are often correlated (Wijnands & van der Klis 1999), both in neutron stars and BHC systems.

In a recent work, Psaltis, Belloni, & van der Klis (1999) (hereafter PBK) have presented a further analogy between

the features observed in neutron star and in BHC systems. Specifically, they have shown that the HBO frequency is apparently correlated with the lower-frequency kHz QPO frequency (Fig. 1 of PBK). With suitable identifications (in part relying upon the break frequency-QPO frequency correlation of Wijnands & van der Klis (1999), as discussed by PBK) to features observed in atoll and BHC systems, this correlation is seen to extend over three decades in Fourier frequency and encompass Z-sources, atoll sources, and BHC sources. If these apparent correlations exist because of an underlying common physical mechanism, then all these variability phenomena are somehow intrinsic to the accretion flow, and do not explicitly rely upon the presence or absence of either a hard surface or a magnetic field in these systems.

A correlation is also observed between the lower-frequency kHz and upper-frequency kHz QPO. Some models (e.g., Miller, Lamb, & Psaltis 1998) associate this difference frequency with being nearly equal to the spin-frequency of the neutron star (in contrast to the theories of Psaltis & Norman, Stella & Vietri 1998, Merloni et al. 1999, and Stella et al. 1999 discussed further below). PBK, however, speculated about whether the observed lower-frequency kHz QPO/upper-frequency kHz QPO correlation would also extend to low frequencies and BHC systems in a manner similar to the putative HBO/lower-frequency kHz QPO correlation. In this work we reexamine a set of observations of the BHC GX 339–4 in order to search for evidence of a “third QPO” in this system. We present such evidence in §2. In §3, we also present evidence for multiple broad-peaked features in the PSD of Cyg X-1. We discuss in §4 the significance of these fits as regards the hypothesized QPO correlations. Furthermore, in light of the observed time lags and degree of linear correlation (i.e., the coherence function) between the soft and hard X-ray variability, we discuss whether the individual “QPO fit-components” to the PSD actually represent physically distinct processes in the accretion flow. We summarize our results in §5.

2 POWER SPECTRAL DENSITIES FOR GX 339–4

In a previous work (NWD), we presented timing analysis for eight separate *RXTE* observations of GX 339–4. The faintest observation, which in terms of 3–9 keV flux is a factor ~ 2.5 fainter than the next brightest observation, clearly shows larger amplitude and characteristically lower-frequency variability than the other observations. Furthermore, the faintest observation shows time lags between its soft and hard X-ray variability (Miyamoto & Kitamoto 1989; Miyamoto et al. 1992; Vaughan & Nowak 1997; Nowak et al. 1999a) that are significantly shorter than those exhibited by the other observations. The remaining observations, which span a factor of ~ 2 in terms of 3–9 keV flux, have relatively similar timing properties. Specifically, the shapes and amplitudes of their PSDs are all comparable, and each shows a narrow PSD peak between 0.26–0.34 Hz. In addition, their Fourier frequency-dependent time lags span less than a factor of two at any given Fourier frequency.

In the frequency range of 0.1–30 Hz, NWD were relatively successful in fitting the PSDs to a functional form

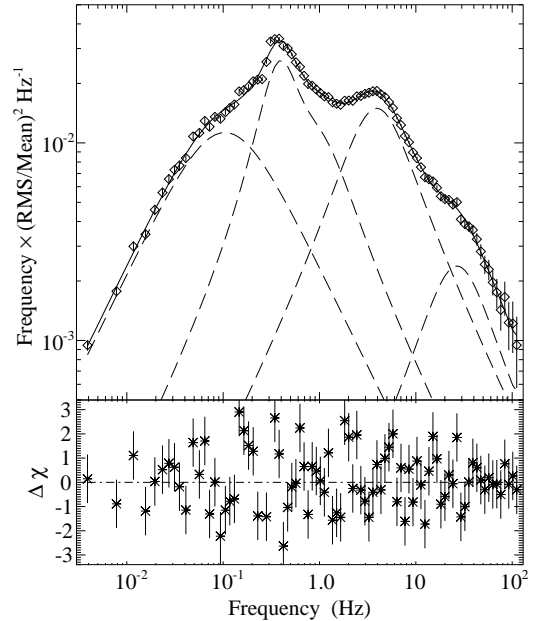


Figure 1. Fourier frequency times composite power spectral density (PSD) of GX 339–4. Thick solid line is the best fit model, whereas the dashed lines are the separate components of the model. The lower panel shows the residuals from the fit.

that consisted of a power law approximately $\propto f^{-1}$, plus two additional Lorentzian components of the form

$$P(f) = \pi^{-1} \frac{R^2 Q f_0}{f_0^2 + Q^2 (f - f_0)^2}, \quad (1)$$

where f_0 is the resonant frequency of the Lorentzian, Q is the quality factor ($\approx f_0/\Delta f$, where Δf is the full-width-half-maximum of the Lorentzian), and R is the fit amplitude (root mean square variability, $\text{rms} = R[1/2 - \tan^{-1}(-Q)/\pi]^{1/2}$, i.e. $\text{rms} = R$ as $Q \rightarrow \infty$). However, due to signal-to-noise considerations, NWD were unable to obtain an adequate fit above ≈ 30 Hz.

As the seven brightest observations of GX 339–4 presented in NWD are so intrinsically similar, we decided to average these observations to form a composite PSD. The PSD, utilizing energy channels covering 0–21.9 keV (i.e., channels A–D from NWD summed) were calculated and averaged together using the normalization of Leahy et al. (1983) (note that this normalization weights the signal PSD by the count rate of the observation, with the average count rates here ranging from 517–877 cps), the noise was subtracted (see Nowak et al. 1999a; and references therein), and then the PSD was renormalized to the normalization of Belloni & Hasinger (1990) using the mean count rate of the summed observations. For this normalization, integrating over Fourier frequency yields the mean square variability relative to the square of the mean of the lightcurve. Error bars on the PSD were calculated as in Nowak et al. (1999a)

We fit this PSD with a model that consisted of a zero frequency-centered Lorentzian ($\equiv A_0/[1 + (f/f_0)^2]$), plus four additional QPO features of the form of eq. 1. The two lowest frequency QPO features were constrained to be harmonics of one another (this allowed us to fit the “asym-

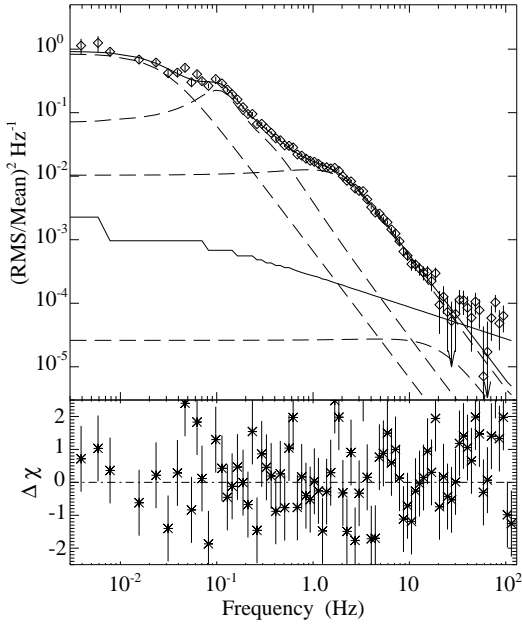


Figure 2. Power spectral density (PSD) of GX 339–4 for the faintest observation presented in Nowak et al. (1999b). Thick solid line is the best fit model, whereas the dashed lines are the separate components of the model. The thin solid line is the residual noise level (see text) after subtracting the mean noise PSD. Lower panel shows the residuals from the fit.

metric” nature of this feature that was commented upon in NWD), but otherwise all QPO amplitudes, widths, and frequencies were allowed to be fit parameters. Our best fit model is also presented in Fig. 1. The fit yielded $\chi^2 = 177$ for 75 degrees of freedom. The fit parameters (with subscripts 0, 1, h, 2, 3, for the zero frequency-centered Lorentzian, lowest frequency QPO, its harmonic, and higher frequency QPOs) are presented in Table 1. Error bars are 90% confidence level, i.e. $\Delta\chi^2 = 2.71$ for one interesting parameter.

We have also applied the above fit to the faintest observation (observation 5) from NWD. Here we are able to fit the zero frequency-centered Lorentzian, the low frequency QPO (plus harmonic), and the middle frequency QPO. The results are also presented in Table 1, and the data are shown in Fig. 2. The high-frequency QPO, if present, is essentially unconstrained (although in Table 1 we give the error bars for the “local minimum” in χ^2). Fig. 2 also shows the residual noise level. This level corresponds to the expected amplitude of positive $1\text{-}\sigma$ fluctuations above the mean value of the Poisson noise PSD, and therefore is indicative of the minimum PSD amplitude at which a signal can be detected (see Nowak et al. 1999a, and references therein). This residual noise level, which scales inversely proportionally to the count rate and to the square root of the integration time, shows the difficulty of detecting the presence of a “third QPO feature” in the high frequency PSD of a single observation. The composite PSD shown in Fig. 1 has a residual noise level ≈ 9 times lower than that for the faintest observation of GX 339–4.

3 POWER SPECTRAL DENSITIES FOR Cyg X-1

Nowak et al. (1999a) discussed observations of Cyg X-1 in its low luminosity/spectrally hard state. In that work, we presented doubly broken power law fits to the PSD, with the low frequency PSD being essentially flat, the middle-frequency PSD being approximately $\propto f^{-1}$, and the high-frequency PSD being approximately $\propto f^{-2}$. Although the *fractional* deviation of the data from the fits was quite small, the reduced χ^2 ranged from $\approx 4\text{--}16$ due to the excellent statistics achievable with RXTE. Here we refit the PSD with the functional form discussed in §2. The fit parameters for two separate energy channels (0–4 keV and 14–45 keV; see Nowak et al. 1999a) are also presented in Table 1, and the fits are shown in Fig. 3.

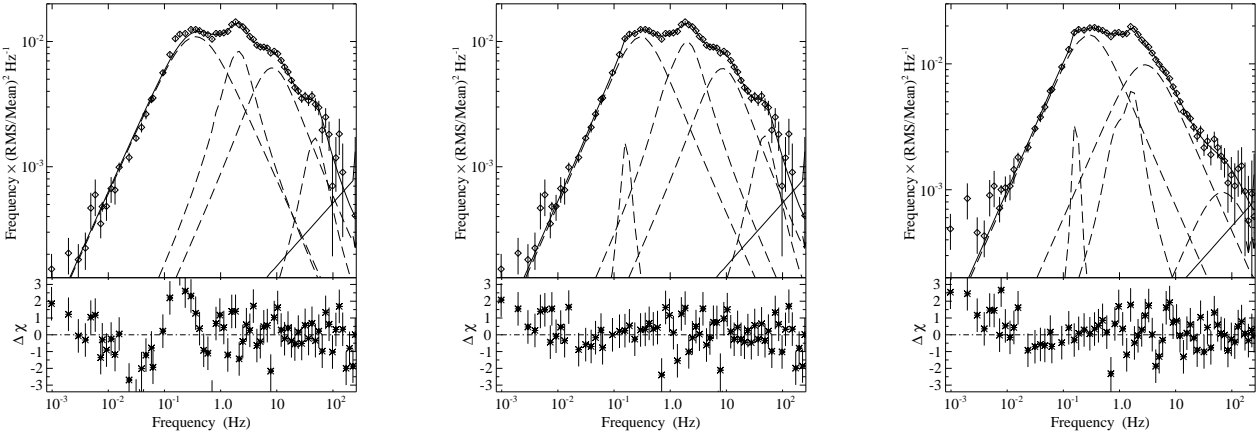
The Cyg X-1 PSDs show subtle, but statistically significant, features. Broad peaks are seen at ≈ 0.3 Hz, 2 Hz, 10 Hz, and 50 Hz. The nearly flat portion of the PSD at $\lesssim 1$ Hz shows some sign of a peak. We use the same model that we fit to GX 339–4, namely a zero frequency-centered Lorentzian, a QPO and its harmonic, plus two additional QPO, and obtain reasonable fits. The reduced χ^2 for these fits were significantly lower ($\Delta\chi^2 > 150$ for eight extra degrees of freedom) than that for the doubly broken power law fits discussed in Nowak et al. (1999a). Note that the lowest frequency ‘QPO’ is identified with the portion of the PSD at $\lesssim 1$ Hz, and its harmonic is identified as having both larger amplitude and greater Q value, in contrast to the fits to GX 339–4.

Although these fits are a significant improvement over the doubly broken power law fits of Nowak et al. (1999a), there are large residuals, especially near 0.2 Hz. We thus considered another fit consisting of five QPO features plus one harmonic (or possibly sub-harmonic, as the QPO associated with the higher of the two related frequencies had a larger amplitude). The results for these fits are presented in Table 2, and the fits are also shown in Fig. 3. This model resulted in significant improvements to the fits ($\Delta\chi^2 \approx 50\text{--}90$, for four extra degrees of freedom); however, compared to the fits presented in Table 1, there was relatively little change in the parameters for the highest frequency QPO fit components.

In these models, what was fit as a zero frequency-centered Lorentzian is now fit as a strong, broad QPO plus a weaker, narrow QPO. Whether these fit components should be regarded as separate physical features, or whether the improvement in the fit is merely an indication of the inadequacy of the zero frequency-centered Lorentzian in describing the low frequency PSD is, of course, unclear. Also along these lines, we note that although we have constrained the features at ≈ 0.8 Hz and 1.6 Hz to be harmonics of each other, the fits are slightly improved ($\Delta\chi^2 = 7.0$ for the 0–4 keV band and $\Delta\chi^2 = 8.9$ for the 14–45 keV band) if the frequencies are allowed to float freely. Note also that there are still positive residuals at $\gtrsim 10^{-3}$ Hz. The above points, as we discuss further below, serve to highlight the fact that when the PSD features are as broad and as subtle as they are in both Cyg X-1 and GX 339–4 the interpretation of what is and is not to be considered a “QPO” becomes much more ambiguous. This needs to be borne in mind in the discussion below of the correlations between fit features.

Table 1. Parameters for PSD Fits. All frequencies are units of Hz.

Observations	zfc-Lorentz.	QPO ₁	QPO _h	QPO ₂	QPO ₃	χ^2/DoF
GX 339-4: Composite of 7 Brightest	$A_0 = 0.22^{+0.01}_{-0.01}$ $f_0 = 0.10^{+0.01}_{-0.01}$	$R_1 = 0.20^{+0.01}_{-0.01}$ $f_1 = 0.34^{+0.01}_{-0.01}$ $Q_1 = 1.7^{+0.2}_{-0.1}$	$R_h = 0.14^{+0.01}_{-0.01}$ $Q_h = 0.9^{+0.2}_{-0.1}$	$R_2 = 0.21^{+0.01}_{-0.01}$ $f_2 = 2.5^{+0.2}_{-0.2}$ $Q_2 = 0.8^{+0.1}_{-0.1}$	$R_3 = 0.08^{+0.01}_{-0.01}$ $f_3 = 18^{+3}_{-4}$ $Q_3 = 0.9^{+0.3}_{-0.2}$	177/75
GX 339-4: Faintest	$A_0 = 0.84^{+0.18}_{-0.15}$ $f_0 = 0.03^{+0.01}_{-0.01}$	$R_1 = 0.19^{+0.04}_{-0.03}$ $f_1 = 0.10^{+0.01}_{-0.02}$ $Q_1 = 1.8^{+0.8}_{-0.7}$	$R_h = 0.16^{+0.17}_{-0.15}$ $Q_h = 0.8^{+0.3}_{-0.3}$	$R_2 = 0.27^{+0.02}_{-0.25}$ $f_2 = 0.9^{+3.5}_{-0.2}$ $Q_2 = 0.5^{+1.9}_{-0.1}$	$R_3 = 0.04^{+0.17}_{-0.04}$ $f_3 = 5^{+19}_{-5}$ $Q_3 = 0.2^{+0.9}_{-0.2}$	80/67
Cyg X-1: 0-4 keV	$A_0 = 0.11^{+0.00}_{-0.01}$ $f_0 = 0.33^{+0.01}_{-0.04}$	$R_1 = 0.02^{+0.08}_{-0.02}$ $f_1 = 0.79^{+0.06}_{-0.09}$ $Q_1 = 2.6^{+1.0}_{-2.6}$	$R_h = 0.09^{+0.02}_{-0.09}$ $Q_h = 2.3^{+3.0}_{-1.0}$	$R_2 = 0.20^{+0.06}_{-0.05}$ $f_2 = 0.7^{+1.3}_{-0.6}$ $Q_2 = 0.3^{+0.2}_{-0.2}$	$R_3 = 0.06^{+0.02}_{-0.05}$ $f_3 = 29^{+33}_{-27}$ $Q_3 = 0.5^{+1.9}_{-0.5}$	126/57
Cyg X-1: 14-45 keV	$A_0 = 0.061^{+0.002}_{-0.002}$ $f_0 = 0.36^{+0.01}_{-0.01}$	$R_1 = 0.003^{+0.011}_{-0.003}$ $f_1 = 0.83^{+0.05}_{-0.05}$ $Q_1 = 1.5^{+6.2}_{-1.4}$	$R_h = 0.13^{+0.01}_{-0.01}$ $Q_h = 1.3^{+0.2}_{-0.2}$	$R_2 = 0.15^{+0.02}_{-0.02}$ $f_2 = 4.2^{+1.3}_{-1.5}$ $Q_2 = 0.6^{+0.2}_{-0.2}$	$R_3 = 0.05^{+0.01}_{-0.01}$ $f_3 = 43^{+6}_{-8}$ $Q_3 = 2.0^{+1.4}_{-0.8}$	154/57

**Figure 3.** Fourier frequency times the power spectral density (PSD) of Cyg X-1 for the 14-45 keV band (left, middle) and the 0-4 keV band (right). Data are the same as presented in Nowak et al. (1999a). Thick solid lines are the best fit models from Table 1 (left) and Table 2 (middle, right), whereas the dashed lines are the separate components of the models. The thin solid lines are the effective noise levels after subtracting the mean noise PSDs. Lower panels show the residuals of the fits.**Table 2.** Parameters for PSD Fits to Cyg X-1 Data. All frequencies are units of Hz.

Component	0-4 keV				14-45 keV			
	R	f	Q	χ^2/DoF	R	f	Q	χ^2/DoF
QPO ₁	$0.29^{+0.02}_{-0.02}$	$0.07^{+0.02}_{-0.06}$	$0.25^{+0.12}_{-0.21}$	71.4/53	$0.22^{+0.01}_{-0.01}$	$0.10^{+0.02}_{-0.03}$	$0.37^{+0.11}_{-0.14}$	65.4/53
QPO ₂	$0.04^{+0.03}_{-0.01}$	$0.17^{+0.01}_{-0.02}$	$12.6^{+51.3}_{-9.8}$		$0.03^{+0.02}_{-0.02}$	$0.16^{+0.01}_{-0.02}$	$6.0^{+24.6}_{-3.7}$	
QPO _{sh}	$0.06^{+0.16}_{-0.05}$	$0.82^{+0.05}_{-0.05}$	$2.3^{+9.4}_{-1.9}$		$0.04^{+0.16}_{-0.04}$	$0.77^{+0.10}_{-0.13}$	$1.9^{+1.8}_{-1.7}$	
QPO ₃	$0.07^{+0.02}_{-0.02}$	—	$3.2^{+2.5}_{-1.0}$		$0.15^{+0.03}_{-0.02}$	—	$1.2^{+0.3}_{-0.3}$	
QPO ₄	$0.23^{+0.04}_{-0.03}$	$0.45^{+0.45}_{-0.40}$	$0.16^{+0.12}_{-0.14}$		$0.15^{+0.02}_{-0.02}$	$4.4^{+1.8}_{-1.7}$	$0.60^{+0.31}_{-0.24}$	
QPO ₅	$0.07^{+0.02}_{-0.03}$	$13.9^{+45.1}_{-12.5}$	$0.21^{+0.85}_{-0.19}$		$0.05^{+0.02}_{-0.01}$	$42.4^{+6.3}_{-9.1}$	$1.9^{+1.2}_{-0.9}$	

4 DISCUSSION

The evidence for a third, high-frequency feature in the composite PSD of GX 339–4 is clear. Removing this feature, the χ^2 increases to 442. Here we should note that to some extent the fits are affected by the fact that separate observations with slightly varying PSD properties have been averaged together. Some broadening of the “QPO features” is expected as a result, and the Q values for features fit to the summed PSD should be considered as lower limits. Likewise, the fitted frequencies and amplitudes of the variability features should be viewed as indicative of an average value, but not strictly applicable to any of the individual PSD used in the combined observation. Furthermore, their error bars should be viewed as lower limits. Along these lines, we note that although the presence of a third feature is indicated, it is almost as well-modelled ($\chi^2 = 207$) by a zero frequency-centered Lorentzian ($\propto [1 + (f/f_b)^2]^{-1}$) with a break frequency of $f_b = 23 \pm 3$ Hz.

The question arises as to what extent this third variability feature might be an artifact of averaging together seven separate observations. This is of some concern; however, we note that in terms of well-measured properties, the seven individual PSDs are very similar to each other. Using the normalization of Belloni & Hasinger (Belloni & Hasinger 1990), at frequencies < 10 Hz (where all seven individual PSDs have good statistics) the variance of the noise subtracted PSDs is $\lesssim 25\%$. Specifically,

$$P_s(f)^{-1} \left(\sum_i [P_s(f) - P_i(f)]^2 \right)^{1/2} \lesssim 0.25, \quad (2)$$

at all frequencies $f \leq 10$ Hz, where $P_i(f)$ are the noise subtracted PSD of the individual observations, and $P_s(f)$ is the noise subtracted PSD of the summed observation. The variance of the mean is lower by a factor of $\sqrt{6}$ and therefore is $\lesssim 10\%$. This result is essentially unchanged if we weight the observations by count rate. The fact that some variation exists from observation to observation means that the error bars that we used should be viewed as lower limits, and the derived χ^2 should be viewed as upper limits. Also as regards possible systematic variations, NWD showed the broad features at ~ 0.35 and 2.5 Hz have fitted frequencies that ranged only from ≈ 0.3 –0.4 Hz and 2–3 Hz, respectively, among the individual observations *and* among separate energy bands within each of these observations. Given the similarities among the PSDs, it would be unusual for the strong third variability feature present in the combined observation to be an artifact of the PSD averaging. (We note that the third variability feature discussed below for Cyg X-1 was for a single, short observation.)

Taking all three features in GX 339–4 as real and not an artifact of the PSD summation, these features are relatively broad (even considering possible systematic broadening due to averaging) compared to high frequency QPO seen, for example, in neutron stars. Statistically, they all have $Q > 0$ at a high significance level; however, they are all far from narrow, periodic features. The QPO at the higher frequency end of the correlation presented by PBK all tend to be much narrower features (in terms of FWHM) than those presented here. Nevertheless, if we take these features and identify the low-frequency QPO with the HBO, the middle-frequency

QPO with the lower-frequency kHz QPO, and the high-frequency QPO with the upper-frequency kHz QPO, then they approximately fall along the correlations suggested by PBK. We show the above data overlaid on the suggested correlation of PBK in Fig. 4. This is true for the composite PSD as well for the PSD of the faintest observation from NWD, keeping in mind that for this latter observation the error bars on the highest frequency feature are for the local minimum and that the presence of this latter feature is not strongly constrained. We also note that the correlation between the frequency, f_0 , of the zero frequency-centered Lorentzian and the frequency, f_1 , of the lowest frequency QPO is in the same sense as the break frequency/QPO frequency correlation discussed by Wijnands & van der Klis (1999).

The fact that the “HBO” and “lower-frequency kHz QPO” of GX 339–4 appear to lie approximately along the suggested correlation was already noted by PBK. What is new here is that there appears to be a third QPO that extends the lower-frequency kHz QPO/upper-frequency kHz QPO correlation downward by nearly two orders of magnitude in Fourier frequency. The high-frequency QPO of GX 339–4 appears to lie slightly below the extrapolation of the lower-frequency kHz QPO/upper-frequency kHz QPO correlation; however, assuming the correlation to be $\propto f^\alpha$, a slope change of $\delta\alpha \sim -0.2$ is all that is required between the low-frequency GX 339–4 point and the high-frequency trend. Furthermore, some theories (e.g., the relativistic precession theory of Stella & Vietri 1998; Merloni et al. 1999; Stella et al. 1999) suggest that one should not expect a single power law over the whole range of the putative correlation. Specific predicted frequency correlations for the relativistic precession theory can be found in Stella et al. (1999).

The features fit to the Cyg X-1 PSD are slightly more problematic to fit onto this trend. In light of the fact that the best fit consists of five QPO features plus one harmonic, there are the questions of which fit components are to be considered as “true QPO” (as opposed to merel a fit artifact) and which are to be associated with which feature in the putative correlation. In Fig. 4, we have taken the fits of Table 2 and associated QPO₅ with the upper-frequency kHz QPO, QPO₄ with the lower-frequency kHz QPO, and QPO₃—the sub-harmonic to the stronger 0.16 Hz feature—with the HBO. With these associations, the features fit to the high energy (14–45 keV) PSD of Cyg X-1 agree with suggested trend, whereas the features fit to the low energy (0–4 keV) PSD of Cyg X-1 deviate from the trend, mostly due to the extremely low frequency of the “lower-frequency kHz QPO”. We note, however, that the frequency-break of this component occurs at roughly the same location in the low and high energy PSDs. The fact that the feature in the low energy PSD has an extremely low $Q \approx 0.2$ leads to a very low fit-frequency in order to yield a break in the same location as the somewhat narrower feature ($Q \approx 0.6$) in the high energy PSD. If one performs a joint fit to the 0–4 keV and 14–45 keV PSDs, constraining the QPO frequencies (but not the amplitudes or widths) to be the same in both bands, a reasonable fit is obtained with $\chi^2 = 156$ for 111 degrees of freedom. The resulting fit frequencies are comparable to the frequencies fit to the 14–45 keV band in Table 2.

It is difficult to test the correlations suggested by PBK since most of the Q values for the fitted features are very

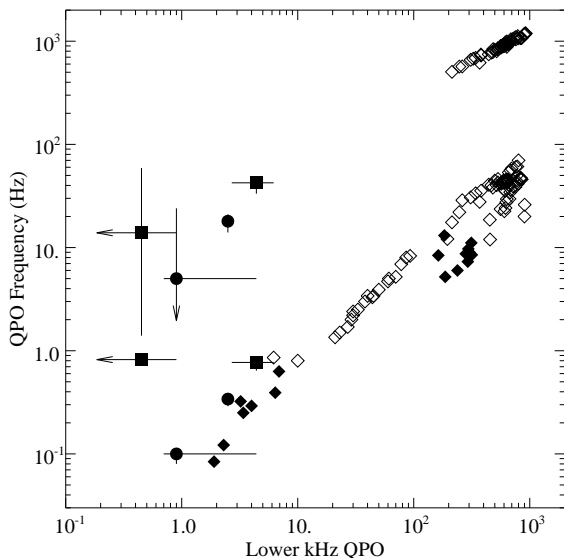


Figure 4. The QPO frequencies presented here (filled circles are for GX 339–4, filled squares are for Cyg X-1), with 90% CL error bars, overlaid on the same graph as presented in Psaltis, Belloni, & van der Klis (1999). Open diamonds correspond to neutron star candidates, filled diamonds to black hole candidates (error bars are not shown for either). Note: QPO identified as “normal branch oscillations” are also shown on this plot (see PBK).

low, making the features very subtle. Another, more serious problem, is the question of identification of the features. One alternative fit to the Cyg X-1 PSDs would be to place a zero frequency-centered Lorentzian with break frequency ≈ 0.01 to remove the low frequency residuals seen in Fig. 3, and then to identify QPO_1 and QPO_2 as the HBO and a harmonic, QPO_3 and QPO_h as the lower-frequency kHz QPO and a harmonic, QPO_4 as the upper-frequency kHz QPO, and QPO_5 as a new, “fourth QPO”. [The theoretical existence of a fourth such frequency has been suggested by Psaltis & Norman (2000), for example.] These frequencies would also fit on the suggested trend of PBK, except now QPO_4 in the low energy PBK would be too low a frequency to fall on the trend for the upper-frequency kHz QPO. *At present, there is no unambiguous, rigorous method of associating a fitted feature with the suggested trend of PBK.*

Even given these caveats regarding correlations between the various fit-components, it is tempting to associate each fit-component of the PSD with a “resonance” in the variability properties of the accretion flow (see Psaltis & Norman 2000). This is counter to the models of Kazanas et al. (1997) and Poutanen & Fabian (1999), for example, that essentially postulate a single “response” for the variability properties of the accreting system. NWD phenomenologically elaborated upon the concept of each PSD fit-component corresponding to a separate physical mechanism by further postulating that each of these system “responses” had a separate “driver”, uncorrelated with the variability-drivers of the other PSD components^{*}. The net Fourier frequency-

^{*} Even if a system has a set of independent responses to a source of input fluctuation or noise, for example the accretion disk re-

sponses discussed by Psaltis & Norman (2000), the net outputs will be perfectly correlated (i.e., have a coherence function of unity) if they are responding to the same source of noise fluctuations. This point is discussed in further detail by Bendat & Piersol (1986), Vaughan & Nowak (1997), and NWD.

† Note that there is still an ambiguity in the values of the Fourier phases, as there are two independent solutions for a two-component fit to the measured phase lag and coherence function. Specifically, see Fig. 8 of NWD, where reflecting the phases of the individual PSD components through the net measured phase lag yields an equally valid solution. In our solution that follows, at low Fourier frequency we choose the phase lag for the zero frequency-centered Lorentzian to be the value closest to the net measured phase lag. Then, progressing to higher Fourier frequencies, we choose solutions that are most nearly continuous with the lower frequency values.

dependent phase lags (or, equivalently, time lags=phase lags/ $2\pi f$) and coherence function [$\gamma^2(f)$, a measure of the degree of *linear* correlation between two lightcurves; see Bendat & Piersol 1986, Vaughan & Nowak 1997] between soft and hard variability were then given by a combination of the phase lags and coherence functions for each individual fit-component of the PSD (see NWD, §4 and Fig. 8; Vaughan & Nowak 1997).

NWD noted that for the case of GX 339–4 wherever one PSD fit component dominated (for example, near 0.3 Hz in Fig. 1, where the low-frequency QPO dominates), the coherence function would be near unity and there would be an approximately flat Fourier phase lag shelf when comparing soft and hard variability. Wherever two PSD fit components crossed one another, there would be a slight dip in the coherence function and a transition from one characteristic Fourier phase lag to another (see Fig. 5). Fig. 1 shows that at any given Fourier frequency, typically two PSD fit components dominate. Ignoring the other two fit components, at any given frequency we can then calculate the phase lag between soft and hard X-ray variability for the remaining two PSD fit components by simultaneously fitting the measured net phase lag and the measured net coherence function[†].

We have carried out such a procedure for the second brightest GX 339–4 observation (which showed the strongest QPO at ≈ 0.3 Hz) presented in NWD. We have fit the 0–21.9 keV PSD of this observation with the same type of model as discussed in Table 1. For this non-composite PSD fit, constraints are again weakest for the “third QPO” fit-component. Furthermore, we have *assumed* this PSD shape and amplitude for both the 0–3.9 keV and 10.8–21.9 keV PSDs. (Fitting each energy band individually, no constraints can be made on the “third QPO”.) We then followed the procedures outlined in §4 of NWD (see specifically eqs. 4 and 5) for fitting the phase lag and coherence function, except that instead of fitting four constant (as a function of Fourier frequency) phases over the entire data set, we fit two phases at any given Fourier frequency. Specifically, at any given Fourier frequency, we fit the phase lags for the two strongest PSD fit-components, *assuming the other two PSD fit components to be negligible*. Error bars do not account for uncertainties in the PSD fit parameters, and only represent that portion of the error due to the uncertainty in the measured phase lag and measured coherence function. The

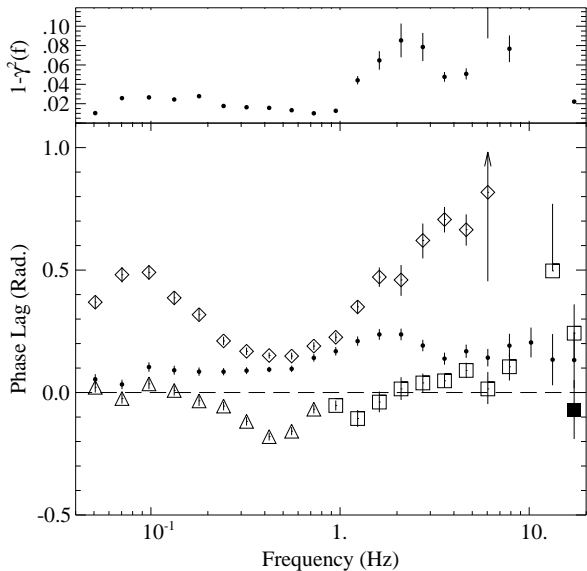


Figure 5. *Bottom Panel:* A possible decomposition of the net Fourier frequency-dependent phase lags between soft (0–3.9 keV) and hard (10.8–21.9 keV) X-ray variability (filled circles) into individual components associated with the PSD fit components shown in Fig. 1. Triangles correspond to the zero frequency-centered Lorentzian, diamonds to the low-frequency QPO (including harmonic), clear squares to the middle-frequency QPO, and filled squares to the high-frequency QPO. Positive values correspond to the hard X-ray variability lagging the soft. *Top Panel:* The coherence function, $\gamma^2(f)$, associated with the net phase lag.

results for this decomposition (which, as we discuss above, is *not* unique) are presented in Fig. 5.

Fig. 5 is presented more for illustrative purposes rather than as a completely rigorous and definitive fit. The things to note about this possible decomposition are the following. If the QPO fit components each represent a separate, independent physical process, then the deviations from unity coherence can be understood within the context of such a model as well. At low frequency the net phase/time lags are most characteristic of the zero frequency-centered Lorentzian, at middle frequencies they are most representative of the low frequency QPO, and at moderately high frequencies they are most representative of the middle frequency QPO. At ≈ 0.3 Hz, there is a recovery of the coherence function to near unity values that would be associated with the low frequency QPO becoming dominant in the PSD. Although it is difficult to accurately measure the high frequency phase/time lags and coherence function, the fact that the middle and high frequency fit components to the PSD have comparable amplitudes at $f \gtrsim 10$ Hz could explain the strong loss of coherence at these frequencies (which is characteristic of Cyg X-1 as well; see Nowak et al. 1999a). Although the net phase lag indicates that hard photons lag the soft photons, it is possible for portions of the individual variability components to show exactly the opposite behavior.

5 SUMMARY

The main results of this work can be summarized as follows.

- A composite power spectrum of GX 339–4 is well-fit by a model that consists of a zero frequency-centered Lorentzian, a moderate width ($Q \sim 1$ –2) quasi-periodic oscillation and its harmonic, plus two additional, broad ($Q \sim 0.5$ –1) QPOs.

- The frequencies of these three QPO components approximately agree with the correlations among horizontal branch oscillations/lower-frequency kHz QPOs/upper-frequency kHz QPOs suggested by Psaltis, Belloni, & van der Klis (1999).

- Fits to the PSD of Cyg X-1 are more problematic. Multiple QPO components provide the best fits to the PSD as a function of observed energy band. Depending upon the identifications made, the high energy band PSD fits can be made consistent with the correlations suggested by Psaltis, Belloni, & van der Klis (1999). The low energy band PSD fits show deviations from these correlations, although a joint fit of the low- and high-energy PSD does allow for a single set of frequencies consistent with the suggested correlations.

- One can construct a phenomenological model where the net Fourier frequency-dependent phase lag and coherence between soft and hard X-ray variability can be expressed as the combination of phase lags and coherences from the individual fit components to the PSD.

- If such a model for the phase lags and coherences is correct, then although the net phase lag indicates that soft variability leads the hard variability, the trend may be exactly opposite for some of the individual variability components. A *requirement* of this model is that although the individual components have coherent variability between soft and hard photons, the variability components are incoherent with one another. This not only requires that each component be representative of a different “response” within the accretion flow, but also that each component has a separate variability “driver”

The correlations between the different fit-components seems at least to be very suggestive. It is tempting to associate all of these quasi-periodic features observed in both neutron star and black hole systems with a common set of phenomena intrinsic to the accretion flow itself, and not to the properties of the compact object such as the presence of a surface or a magnetic field. Such may not be the case in reality, however. The presence of what appear to be four distinct features (the zero frequency-centered Lorentzian and three broad, quasi-periodic features) in the PSD of GX 339–4, coupled with suggestive evidence from the Fourier frequency-dependent phase lags and coherence function (see also NWD), at the least seems to be arguing for models with multiple, distinct sources of variability (e.g., Psaltis & Norman 2000), and against models with a single “type” of variability (e.g., Kazanas et al. 1997, Poutanen & Fabian 1999).

This research has been supported by NASA grants NAG5-3225 and NAG5-4731. Dimitrios Psaltis kindly provided the data for Fig. 4 and valuable comments. I also would like to thank Andrew Hamilton for useful discussions, the hospitality of the Aspen Center for Physics, the participants of the “X-ray Probes of Relativistic Astrophysics” workshop for many useful and stimulating discussions, and the hospitality of P. Coppi, C. Bailyn, and the Yale Astronomy department while this work was being completed.

REFERENCES

- Belloni T., Hasinger G., 1990, *A&A*, 227, L33
- Bendat J., Piersol A., 1986, *Random Data: Analysis and Measurement Procedures*, Wiley, New York
- Hasinger G., van der Klis M., 1989, *A&A*, 225, 79
- Homan J., van der Klis M., Wijnands R., et al., 1998, *ApJ*, 499, L41
- Kazanas D., Hua X.M., Titarchuk L., 1997, *ApJ*, 480, 280
- Klis M.v., 1995, Black-hole binaries. in Lewin W.H.G., van Paradijs J., van den Heuvel E.P.J., eds, *X-Ray Binaries*. Cambridge Univ. Press, Cambridge, Ch. 4, p. XXX
- Leahy D.A., Darbro W., Elsner R.F., et al., 1983, *ApJ*, 266, 160
- Merloni A., Vietri M., Stella L., Bini D., 1999, *MNRAS*, 304, 155
- Miller M.C., Lamb F., Psaltis D., 1998, *ApJ*, 508, 791
- Miyamoto S., Kitamoto S., 1989, *Nature*, 342, 773
- Miyamoto S., Kitamoto S., Iga S., et al., 1992, *ApJ*, 391, L21
- Nowak M.A., Vaughan B.A., Wilms J., et al., 1999a, *ApJ*, 510, 874
- Nowak M.A., Wilms J., Dove J.B., 1999b, *ApJ*, 517, 355
- Poutanen J., Fabian A.C., 1999, *MNRAS*, 306, 31p
- Psaltis D., Belloni T., van der Klis M., 1999, *ApJ*, 520, 262
- Psaltis D., Norman C., 2000, *ApJ* in press
- Stella L., Vietri M., 1998, *ApJ*, 492, L59
- Stella L., Vietri M., Morsink S., 1999, *ApJ*, 524, L63
- Strohmayer T., Zhang W., Swank J., et al., 1996, *ApJ*, 469, L9
- van der Klis M., 1994a, *A&A*, 283, 469
- van der Klis M., 1994b, *ApJS*, 92, 511
- van der Klis M., Swank J., Zhang W., et al., 1996, *ApJ*, 469, L1
- Vaughan B.A., Nowak M.A., 1997, *ApJ*, 474, L43
- Wijnands R., van der Klis M., 1999, *ApJ*, 514, 939